AD_____

Award Number: DAMD17-01-1-0226

TITLE: New Approaches in SPECT Breast Imaging

PRINCIPAL INVESTIGATOR: Kelly E. Braun
R. Jaszczak, Ph.D.
K. Bobkov, Ph.D.
J. Bowsher, Ph.D.

CONTRACTING ORGANIZATION: Duke University
Durham, NC 27708-0077

REPORT DATE: July 2005

TYPE OF REPORT: Annual Summary

PREPARED FOR: U.S. Army Medical Research and Materiel Command
Fort Detrick, Maryland 21702-5012

DISTRIBUTION STATEMENT: Approved for Public Release;
Distribution Unlimited

The views, opinions and/or findings contained in this report are those of the author(s) and should not be construed as an official Department of the Army position, policy or decision unless so designated by other documentation.

REPORT DOCUMENTATION PAGE

1. REPORT DATE (DD-MM-YYYY)	2. REPORT TYPE	3. DATES COVERED (From - To)
01-07-2005	Annual Summary	1 Jul 2001 - 30 Jun 2005

4. TITLE AND SUBTITLE
New Approaches in SPECT Breast Imaging

5a. CONTRACT NUMBER

5b. GRANT NUMBER
DAMD17-01-1-0226

5c. PROGRAM ELEMENT NUMBER

6. AUTHOR(S)
Kelly E. Braun

R. Jaszczak, Ph.D.
K. Bobkov, Ph.D.
J. Bowsher, Ph.D.
E-Mail: keb21@duke.edu

5d. PROJECT NUMBER

5e. TASK NUMBER

5f. WORK UNIT NUMBER

7. PERFORMING ORGANIZATION NAME(S) AND ADDRESS(ES)

Duke University
Durham, NC 27708-0077

8. PERFORMING ORGANIZATION REPORT NUMBER

9. SPONSORING / MONITORING AGENCY NAME(S) AND ADDRESS(ES)
U.S. Army Medical Research and Materiel Command
Fort Detrick, Maryland 21702-5012

10. SPONSOR/MONITOR'S ACRONYM(S)

11. SPONSOR/MONITOR'S REPORT NUMBER(S)

12. DISTRIBUTION / AVAILABILITY STATEMENT
Approved for Public Release; Distribution Unlimited

13. SUPPLEMENTARY NOTES
Original contains color plates: All DTIC reproductions will be in black and white.

14. ABSTRACT
Abstract follows.

15. SUBJECT TERMS
Nuclear medicine, single photon emission computed tomorgraphy (SPECT), OSEM, filtered backprojection, breast imaging, Orlov

16. SECURITY CLASSIFICATION OF:			17. LIMITATION OF ABSTRACT	18. NUMBER OF PAGES	19a. NAME OF RESPONSIBLE PERSON
a. REPORT	b. ABSTRACT	c. THIS PAGE			19b. TELEPHONE NUMBER (include area code)
U	U	U	UU	24	

ABSTRACT

The primary objective of this research is to develop new techniques in single photon emission computed tomography (SPECT) breast cancer imaging providing improved detection and characterization of early stage breast cancer. Projection data were acquired by implementing a tiltable SPECT system on a breast and torso phantom. The data were reconstructed with both an ordered subset expectation maximization (OSEM) algorithm and a filtered backprojection (FBP) algorithm with a ramp filter. Results indicated that the OSEM values for SNR and contrast were higher at all tilt angles and may offer better shape and uniform activity distribution of the breast compared to FBP images. Also, by using a tilted head SPECT system, the radius of rotation decreases and the chest wall near the breast can be adequately imaged. This results in increased resolution and sensitivity. A pinhole collimator is advantageous in imaging a breast due to its ability to get close to the breast and achieve a small radius of rotation, though lead shielding was ineffective in eliminating background activity from the myocardium and liver. Statistical analysis of differing acquisition geometries for incomplete circular orbits for breast pinhole SPECT imaging have shown greater reduction in sampling artifacts.

Table of Contents

INTRODUCTION

The primary objective of this research centered around breast cancer imaging, specifically developing new techniques in single photon emission computed tomography (SPECT) breast cancer imaging which will provide improved detection and characterization of breast cancer. A leading hypothesis in this research is that by using a vertical axis of rotation (VAOR) and various camera head and pinhole collimator configurations, several advantages can be gained over traditional horizontal axis of rotation (HAOR) SPECT. A tiltable head SPECT (TH-SPECT) system allows for improved imaging of lesions closer to the chest wall as well as a smaller radius of rotation [1]. Compared to a filtered backprojection reconstruction algorithm, OSEM reconstruction algorithm displayed improved images [3]. To improve contrast and signal-to-noise (SNR) values, the effect of shielding the patient bed with lead was investigated [4]. A statistical analysis of incomplete circular orbits for breast pinhole SPECT imaging was conducted, resulting in the reduction of sampling artifacts by more nearly satisfying the Tuy complete-sampling requirement [5]. Due to the fact that regions of the breast-torso interface are often times not adequately sampled, the potential of body-contour and lung-boundary information was considered for reducing incomplete-sampling artifacts [6].

BODY

Disadvantages of HAOR breast imaging with SPECT include attenuation through the torso and a large radius of rotation (ROR). Tilting a camera head allows the collimator to get closer to the breast and chest wall. Using various tilt angles for the camera heads, an axially Tiltable 2-Headed SPECT (TH-SPECT) system was used to observe resolution, contrast and SNR values in fillable breast and torso phantoms containing a 1 cm lesion suspended in the breast. The results of this HAOR TH-SPECT system were compared to high-count planar images. An ordered subsets expectation maximization (OSEM) algorithm (8 subsets, 3 iterations), which accounted for the geometry of the system, was used to reconstruct the data. In comparison to the high count planar images, a 0.5mL lesion was more clearly visible in TH-SPECT. Lesion contrast and lesion SNR improved nearly three and two times, respectively. As a result, this system configuration reduced the radius of rotation and allowed for adequate imaging near the chest wall breast tissue, improving sensitivity and resolution [1]. The one drawback to this system is the fact that axially blurring affects the chest wall region of the breast. Future work could be done with a combination of two heads tilting at different angles, aiming to provide more complete sampling. The manuscript detailing this experiment was submitted with last year's annual summary.

One concern dealing with TH-SPECT that was evident in the previous study dealt with insufficient axial sampling of the image space. Specifically, insufficient sampling of the myocardium, liver and torso will cause interference when imaging small lesions in the breast and thus result in artifacts in the reconstructed images. Tilting the camera head prevents the reconstruction algorithms from meeting the Orlov sphere requirement, which states that an image space must be sampled over a great circle [2]. A three-dimensional algorithm is needed to reconstruct TH-SPECT data. Iterative methods, such as OSEM, have been used to model the sampling of frequency space associated with circular orbits with a tilted geometry. A filtered backprojection (FBP) algorithm was devised with the intent of successfully reconstructing tilted-head geometries. This FBP method was compared to OSEM for a fillable breast phantom containing lesions at various tilt angles and for a fillable breast

phantom containing a mini-Defrise disk imaged with parallel-beam TH-SPECT at angles of 0-15 degrees. Values for both contrast and SNR were compared. The publication supporting this research can be found in the appendix. In this paper [3], a geometric derivation of the ramp filter is presented for tilted parallel beam geometries. Using this ramp filter, a FBP method was implemented and compared with an iterative OSEM algorithm using TH-SPECT data. The FBP results indicated a greater increase in backprojection artifacts with greater angular tilt, as well as a greater bias in FBP noise versus bias plots with a greater angular tilt. OSEM reconstructions showed greater SNR and contrast values at all tilt angles [3]. Because TH-SPECT data do not sufficiently sample the Orlov sphere, artifacts are present in all reconstructions. However, OSEM TH-SPECT reconstruction offers better shape and uniform activity distribution of the breast compared to FBP methods [3]. This paper was also submitted with last year's annual summary report.

A pinhole collimator is advantageous over a parallel-hole collimator in imaging the breast in its ability to decrease the ROR, resulting in better resolution for detecting lesions. However, an issue in both parallel and pinhole SPECT breast imaging is photon contamination from other organs that will impact the clarity of the image, such as the liver, myocardium, lungs and gall bladder. Since a pinhole collimator, due to its geometry, will collect fewer photons from the torso, the hypothesis that we set out to prove was that lead shielding on the bed would further reduce the unwanted photons from outlying organs that were collected by the pinhole collimator and thus increase the contrast and SNR of the image. The manuscript detailing our experiment more fully has been attached in the appendix [4]. Using a Trionix XLT scanner (Trionix Research
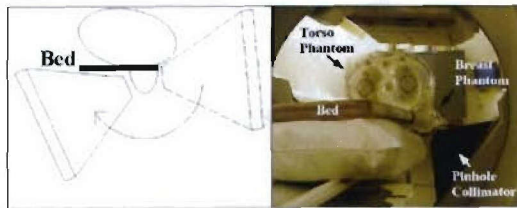

Figure 1

Lab, Twinsburg, Ohio) with one pinhole collimator, experimental data was obtained of a breast phantom mounted on an anthropomorphic torso phantom placed in a prone position on the bed (Figure 1). The first set of scans consisted of the torso phantom and all its organs filled with activity, and the second set of scans consisted of the same configuration of the torso phantom as the first scan, except with the addition of lead shielding placed over the entire table except for where the breast was located. The angular range of these scans was 186 degrees, resulting in an incomplete circular orbit (ICO). The breast contained two spherical lesions (1.6 cm diameter), both of which were filled with activity. The projection data were reconstructed, without shielding attenuation modeling or scattering and attenuation correction, with an OSEM algorithm having thirty iterations and eight subsets. A 3-D region-of-interest analysis was performed on the lesions to evaluate shielding effects. The use of shielding slightly reduced noise in contrast estimates, from about 0.25 to 0.23. However, shielding increased bias in contrast from 0.24±0.08 to 0.44±0.07. SNRs were also lower with shielding. These results suggest that if shielding is to be of benefit, shielding attenuation must be modeled within iterative reconstruction. However, the standard reconstruction algorithms such as OSEM and MLEM are limited in reconstructing inconsistent projection data.

Using the suggestion that pinhole collimation may provide an effective tool for characterization of small lesions within the breast because it yields higher resolution and sensitivity, clinical count density scans were used to quantitatively analyze the effects of three different acquisition geometries. The torso generally limits the angular range of the pinhole collimator, making it virtually impossible to completely sample the entire breast volume and thus

satisfy the Tuy complete sampling requirement [5]. Thus, we present these three novel orbits in an attempt to fully sample the breast volume: single half-circular orbit, three parallel half circles separated axially, and three half circles with the plane of rotation for two half circles tiled +30 and -30 degrees relative to the middle. Additional details can be found in the attached manuscript [5]. The results suggested that triple half circular orbits are superior to the single half circular orbit [5]. Attenuation and scatter corrections, which will change total counts in ROI's, were not taken into consideration. Single half circular orbits and triple half circular orbits can be readily implemented on a standard clinical scanner.

With the proposal of vertical axis of rotation (VAOR) breast imaging, the pinhole collimator orbits around the breast rather than about the torso, avoiding attenuation through the body. As with VAOR, tilting the gamma camera can also increase projection sampling near the breast-torso interface. However, the sampling near the breast-torso interface tends to be limited, and the estimated radiotracer distribution in these important regions can be highly distorted, resulting in artifacts near this interface and in the axilla, regions which are important for the diagnosis of breast cancer [6]. By obtaining patient-contour and lung-boundary information, the estimation of SPECT radiotracer distribution may be improved. A more detailed description of this idea can be found in the attached manuscript [6].

KEY RESEARCH ACCOMPLISHMENTS

- Statistical analysis of differing incomplete circular orbits for breast pinhole SPECT imaging [5].
- Completed comparison of contrast and SNR values between shielded and unshielded torso phantom [4].
- Analysis of body-contour and lung-boundary information for reduced incomplete-sampling artifacts [6].
- Development and evaluation of FBP TH-SPECT image reconstruction algorithm using a geometric derivation of the ramp filter [3].
- Comparison of FBP TH-SPECT algorithm with traditional FBP and OSEM [3].
- Acquisition, evaluation, and comparison of TH-SPECT data, including contrast and S/N analysis using experimental phantoms [1].
- Acquisition and evaluation of combined horizontal and vertical axes of rotation.
- Design of special adapter plate for using Triad XLT pinhole collimator on T22 SPECT system.

REPORTABLE OUTCOMES:

Manuscripts

- Lee T, Braun K, Jazczak J, Bowsher J, Bobkov K, The Effects of Lead Shielding of Background Organ Activity in Pinhole Single Photon Emission Computed Tomography (SPECT) Breast Tumor Imaging, *2004 IEEE Nuclear Science Symposium & Medical Imaging Conference*, 16-21 October, 2004, Rome, Italy.

- Bobkov K, Bowsher J, Greer K, Jaszczak R, Braun K, Lee T, "Statistical Analysis of Incomplete Circular Orbits for breast Pinhole SPECT Imaging," *2004 IEEE Nuclear Science Symposium & Medical Imaging Conference*, 16-21 October, 2004, Rome, Italy.
- Bowsher J, Lee T, Braun K, Bobkov K, Jaszczak R, "Reduced Incomplete-Sampling Artifacts in Pinhole SPECT Breast Imaging Using Body-Contour and Lung-Boundary Constraints," *2004 IEEE Nuclear Science Symposium & Medical Imaging Conference*, 16-21 October, 2004, Rome, Italy.

CONCLUSIONS

From the above research, several conclusions can be drawn. To combat the issue of insufficient sampling, it was shown that an OSEM algorithm will reconstruct the projection data better than a FBP, showing greater SNR and contrast values at all tilt angles. Also, more elaborate orbits may provide a more complete sampling of the breast volume. To combat the issues produced by a HAOR, the camera heads were tilted, reducing the radius of rotation and allowing for adequate imaging near the chest wall breast tissue. The combination of an OSEM algorithm and TH-SPECT data offers better shape and uniform activity distribution of the breast, improving contrast and lesion SNR. Concerning the lead shielding, comparison of contrast and SNR between shielded and non-shielded images revealed that contrast and SNR is significantly lower with lead shielding than without lead shielding, the opposite of what we had expected. And finally, to better assess the breast-torso interface, it was demonstrated that obtaining lung-boundary information and body contour information will improve the estimation of the radiotracer distribution within that area.

REFERENCES

[1]   Pieper BC, Bowsher JE, Tornai MP, Peter J, Greer K, Jaszczak JJ, "Breast Tumor Imaging Using Tiltable Head SPECT Cameras," *IEEE Trans. Nucl. Sci.*, vol. 48, pp. 1477-1482, Aug 2001.

[2]   Orlov SS, "Theory of Three Dimensional Reconstruction," *Sov. Phys. Crystallogr.*, vol. 20, no. 3, pp. 312-314, 1975.

[3]   Pieper BC, Bowsher JE, Tornai MP, Archer CN, Jaszczak JJ, "Parallel-Beam Tilted-Head Analytic SPECT Reconstruction: Derivation and Comparison with OSEM," *IEEE Trans. Nucl. Sci.*, vol. 49, pp. 2394-2400, Oct 2002.

[4]   Lee T, Braun K, Jazczak J, Bowsher J, Bobkov K, "Effects of Lead Shielding of Background Organ Activity in Pinhole SPECT Breast Tumor Imaging," *2004 IEEE Nuclear Science Symposium & Medical Imaging Conference*, 16-21 October, 2004, Rome, Italy.

[5]   Bobkov K, Bowsher J, Greer K, Jaszczak R, Braun K, Lee T, "Statistical Analysis of Incomplete Circular Orbits for Breast Pinhole SPECT Imaging," *2004 IEEE Nuclear Science Symposium & Medical Imaging Conference*, 16-21 October, 2004, Rome, Italy.

[6]   Bowsher J, Lee T, Braun K, Bobkov K, Jaszczak R, "Reduced Incomplete-Sampling Artifacts in Pinhole SPECT Breast Imaging Using Body-Contour and Lung-Boundary Constraints," *2004 IEEE Nuclear Science Symposium & Medical Imaging Conference*, 16-21 October, 2004, Rome, Italy.

APPENDICES

[1]   Lee T, Braun K, Jazczak J, Bowsher J, Bobkov K, "Effects of Lead Shielding of Background Organ Activity in Pinhole SPECT Breast Tumor Imaging," *2004 IEEE Nuclear Science Symposium & Medical Imaging Conference*, 16-21 October, 2004, Rome, Italy.

[2]   Bobkov K, Bowsher J, Greer K, Jaszczak R, Braun K, Lee T, "Statistical Analysis of Incomplete Circular Orbits for Breast Pinhole SPECT Imaging," *2004 IEEE Nuclear Science Symposium & Medical Imaging Conference*, 16-21 October, 2004, Rome, Italy.

[3]   Bowsher J, Lee T, Braun K, Bobkov K, Jaszczak R, "Reduced Incomplete-Sampling Artifacts in Pinhole SPECT Breast Imaging Using Body-Contour and Lung-Boundary Constraints," *2004 IEEE Nuclear Science Symposium & Medical Imaging Conference*, 16-21 October, 2004, Rome, Italy

The Effects of Lead Shielding of Background Organ Activity in Pinhole Single Photon Emission Computed Tomography (SPECT) Breast Tumor Imaging

T. Lee, *Member, IEEE*, K. Braun, *Member, IEEE*, R. Jaszczak, *Fellow, IEEE*, J. Bowsher, *Member, IEEE*, K. Bobkov

Abstract—The objective of this study was to investigate the effect on contrast and SNR (Signal-to-Noise Ratio) of shielding the patient bed with lead. Shielding reduces other-organ photon contamination, but may result in incomplete sampling of other organs and increased data inconsistency, if shielding attenuation is not modeled during reconstruction. A Trionix XLT scanner with one pinhole collimator was used to obtain experimental data on a breast phantom mounted on a torso phantom. The torso phantom contained the liver, lungs, and myocardium, all filled with varying amounts of 99mTc-MIBI. The breast phantom contained two spherical lesions, also filled with 99mTc-MIBI. The bed contained a cut-out for the prone breast attachment. Ten scans were performed with bed shielding, and without, in order to determine the statistical significance of the analysis. The incomplete circular orbit angular range was 186 degrees and consisted of 94 views with a 2 degree step between each view. The data were then reconstructed by OSEM with 8 subsets, using up to 30 iterations without modeling shielding attenuation. A 3-D region-of-interest analysis was performed on a lesion to evaluate shielding effects. Post-filtering was applied for better image quality. The use of shielding slightly increased noise in contrast estimates, from about 0.25 to 0.30. In addition, shielding increased bias in contrast from 0.1+/-0.08 to 0.5+/-0.09. For a given cutoff frequency, SNR is lower with shielding than without. These results suggest that if shielding is to be of benefit, shielding attenuation must be modeled within iterative reconstruction.

I. INTRODUCTION

Nuclear imaging using Single Photon Emission Computed Tomography (SPECT) has recently emerged as an imaging modality used to image the functional activity of a human organ or a cancer. The possible utility of a SPECT imaging approach in breast cancer management is its potential to differentiate between benign and malignant cancers [1]. 99mTc-MIBI concentrates strongly in malignant breast cancers [2], however, the soft tissue around the lesion contributes scattering to the image, often causing smaller malignant lesions to go undetected and decreasing the image quality.

When imaging a breast with a large field-of-view camera, a pinhole collimator is advantageous in its ability to decrease the radius-of-rotation (ROR) and get close to the breast, though only an incomplete circular orbit is possible due to interference between the phantom and the pinhole collimator. Due to the need of a pinhole collimator to be as close as possible to the object of interest, sensitivity decreases and attenuation increases when imaging through the backside of the torso. It has been shown that SPECT imaging of a breast phantom using a pinhole collimator has significantly reduced the effects of scattering from breast tissue surrounding the lesion [1]. However, when the breast is mounted on an anthropomorphic torso phantom, increased scattering is introduced from the myocardium, liver and gall bladder that may impact the clarity of the breast image. The use of a pinhole collimator may obtain data with decreased photon contamination from these organs.

Although the organ of interest is the breast, the myocardium, liver, and gall bladder also take up the 99mTc-MIBI. Thus, in our phantom studies, we are investigating the difference that lead shielding will make in the contribution of photons from the outlying organs that are collected through the breast phantom by the pinhole collimator. More specifically, we are interested in determining how the radioactivity uptake in these organs affects the contrast, bias and SNR in the phantom breast images using a region-of-interest (ROI) analysis.

II. DATA ACQUISITION

A Trionix XLT scanner (Trionix Research Lab, Twinsburg, Ohio) with one pinhole collimator was used to obtain the experimental data on a breast phantom mounted on an anthropomorphic torso phantom placed in a prone position on the bed. Two sets of scans were performed, each containing 10 individual scans. The first set of scans consisted of the torso phantom and all its organs filled with activity as shown in Fig.1.
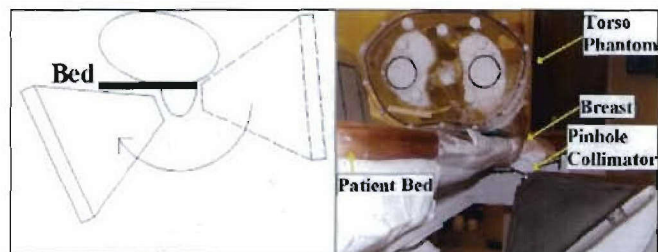
Fig. 1. A) ICO angular range B) Experimental Setup
The center of rotation of the camera was at the center of the breast. The angular range of the ICO was limited by the patient bed and the torso phantom because the pinhole collimator would collide with the torso on one side and the bed on the other.

The second set of scans consisted of the same configuration of the torso phantom as the first scan, except with the addition of lead sheets of thickness 5mm placed over the entire table except for where the breast was located, as shown in Fig. 2.

Fig. 2. A) Without Shielding B) With Shielding
5mm lead sheets were placed on the patient bed to simulate shielding. A ceiling mounted laser projected an x-y plane onto the dorsal side of the phantom, allowing for the accurate repositioning of the torso between scans.

These scans had an angular range from 106° to 292°. All the scans consisted of an ROR of 12.9 cm, a tungsten pinhole aperture of 3 mm, and a pinhole focal length of 20 cm. All the scans consisted of 94 views with 2° steps between each view. The scan time per view for the first scan was 3 seconds. The scan time per view for each scan thereafter was adjusted in length for radioactive decay so that the effective scan times were the same for all scans. A total of 20 scans were performed. Ten scans of each configuration were performed to obtain a statistical ensemble for a more complete statistical analysis. The projection data was stored in a grid size of 256x128 (pixel size = 1.72 mm) for further processing.

A. Phantom Study

The torso phantom (Model ECT/TOR/P, Data Spectrum, Corp., Hillsborough, NC) contained the lungs, liver, and heart as shown in Fig. 3. The breast was mounted on the left side of the torso and placed in a prone position on the imaging bed. Two hollow spheres, used to simulate lesions, were placed in the breast, one approximately three centimeters below the nipple and the other close to the chest wall towards the sternum. Both had an outside diameter of 2.2 cm. This relatively large sphere size was chosen in order to assist with positioning the ROI's in the reconstructed image. The liver (volume =1180 mL) was filled with 22.5 µCi/mL, the myocardium (volume = 118 mL) was filled with 30 µCi/mL, and the lesions (volume = 5.5 mL) were filled with 7.5 µCi/mL. The remaining parts of the torso and breast, the ventricle, and the lungs were filled with 1.5 µCi/mL [3]. This is depicted in tabular form in Table 1. To expedite the scanning time, increased concentrations above normal clinical concentrations were used.

Table 1
Radioactivity in the torso phantom

	Radioactivity (µCi/mL)
Liver	22.5
Myocardium	30
Lesions (2)	7.5
Others	1.5
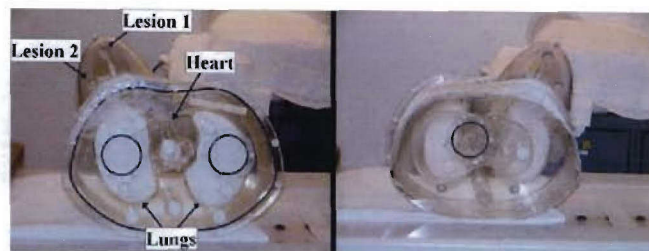
Fig. 3. A) Anterior View B) Posterior View
These views show the location of all the organs that were filled with activity in these scans.

B. Data Processing

In this initial study, the projection data were reconstructed, without shielding attenuation modeling or scattering and attenuation correction, with OS-EM (Ordered Subset Expectation Maximization) algorithm for faster processing with minimal image quality compensation. Thirty iterations with an OS level (i.e. the number of ordered subsets) of 8 were used over 94 projection views. The reconstructed image was in a grid size of 128x128x100 with a voxel size of 2 mm.

III. RESULTS AND DISCUSSIONS

The reconstructed images for individual scans were relatively noisy making ROI visualization rather difficult. One method to overcome this difficulty was to sum up all the

individual scans for each set before reconstruction to simulate a long scan, assuming that the phantom did not move during data acquisition. The simulated long scan provided for easier ROI visualization since noise was reduced. This is shown in Fig. 4. Comparison of the profiles along the white line shows that the individual scan is noisier than the long scan.
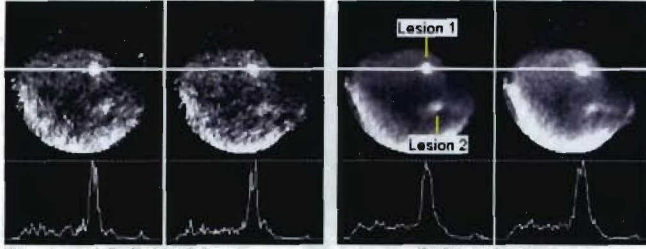
Fig. 4. A) Individual Scans   B) Long Scans
a)Without shielding b)With shielding c)Without Shielding d)With shielding Detection of difference between shielded scan and non-shielded scan is visually difficult both in individual and long scans. Lesion 2 in individual scan is difficult to visualize. Lesion 2 exhibits distortion from incomplete sampling.

A. Determination of ROI

The sphere closer to the chest wall was distorted in shape after reconstruction, most likely due to insufficient sampling. The circled lesion closer to the nipple, shown in Fig. 5, is used for analysis. A spherical ROI of 0.9 cm in radius was created within the lesion volume with its center at the centroid of the lesion. Statistical evaluation was highly dependent upon where the background was because scattering and attenuation were not corrected in the image. To achieve uniformity, a background mask was obtained by creating a shell of 1.2 cm in thickness around the sphere ROI with a gap of 0.8 cm between the surface of the ROI mask and the inner surface of the background shell. This is shown in Fig. 5.

Fig. 5. Determining Signal ROI and Background ROI. The mask developed for the lesion was applied to both the shielded and the non-shielded images. The same method of using an annular ring around the lesion for determining the background ROI was also used for both shielded and non-shielded images.
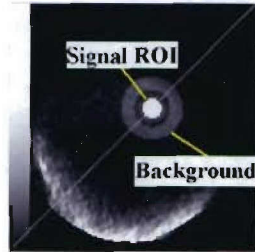
B. ROI Analysis

Contrast is the difference in the image gray scale between closely adjacent regions on the image and signal-to-noise ratio (SNR) is the amount of signal in an image in relation to the amount of noise. Both of these values were employed to evaluate shielding effects. They were computed as follows:

$$Sig = |\overline{S} - \overline{B}| \quad (1)$$

$$C = \frac{Sig}{\overline{B}} \quad (2)$$

$$\hat{C} = \frac{\sum_{i=1}^{N} C_i}{N} \quad (3)$$

$$\sigma_{\hat{C}} = \sqrt{\frac{\sum_{i=1}^{N} (C_i - \hat{C})^2}{N-1}} \quad (4)$$

$$\overline{Sig} = \frac{1}{N} \sum_{i=1}^{N} Sig_i \quad (5)$$

$$\sigma_{\overline{Sig}} = \sqrt{\frac{\sum_{i=1}^{N} (Sig_i - \overline{Sig})^2}{N-1}} \quad (6)$$

$$SNR = \frac{\overline{Sig}}{\sigma_{\overline{Sig}}} \quad (7)$$

where $\overline{S}$ is the mean pixel intensity in the signal ROI and $\overline{B}$ is the mean pixel intensity in the background ROI. For all scans in each data set, individual contrast is calculated using Equation 2. The ensemble contrast ($\hat{C}$) is the ensemble mean of the individual scans shown in Equation 3. Noise ($\sigma_{\hat{C}}$) is the standard deviation from which the ensemble contrast ($\hat{C}$) arises (Equation 4). Standard Error (SE) of the mean is obtained by dividing the Noise ($\sigma_{\hat{C}}$) by $\sqrt{N}$, where N is the number of scans in each set. Bias is the difference between the measured contrast and true contrast ($C_{true} = 4$). Finally, SNR is the ratio of $\overline{Sig}$ to $\sigma_{\overline{Sig}}$, where $\overline{Sig}$ is the ensemble difference between $\overline{S}$ and $\overline{B}$, and $\sigma_{\overline{Sig}}$ is the noise of the ensemble. The results are tabulated in Table 2 and plotted in Fig. 6.

Table 2
Shielding and no shielding table without filtering

	Without Shielding - No Filter Applied			
	Contrast			SNR
Iteration	Mean	Noise	Bias	Mean
1st	3.8±0.07	0.23	0.2±0.07	14.6
2nd	4.3±0.07	0.24	0.3±0.07	17.8
3rd	4.2±0.07	0.22	0.2±0.07	17.8
5th	4.2±0.08	0.24	0.2±0.08	17.6
10th	4.1±0.08	0.25	0.1±0.08	17.5
15th	4.1±0.08	0.26	0.1±0.08	17.5
20th	4.1±0.08	0.26	0.1±0.08	17.5
30th	4.1±0.08	0.26	0.1±0.08	17.5
	With Shielding - No Filter Applied			
	Contrast			SNR
Iteration	Mean	Noise	Bias	Mean
1st	3.4±0.09	0.27	0.6±0.09	15.3
2nd	3.8±0.1	0.3	0.2±0.1	18.3
3rd	3.8±0.09	0.29	0.2±0.09	18.5
5th	3.8±0.1	0.3	0.2±0.1	18.4
10th	3.8±0.1	0.31	0.2±0.1	18.3
15th	3.8±0.1	0.32	0.2±0.1	18.3

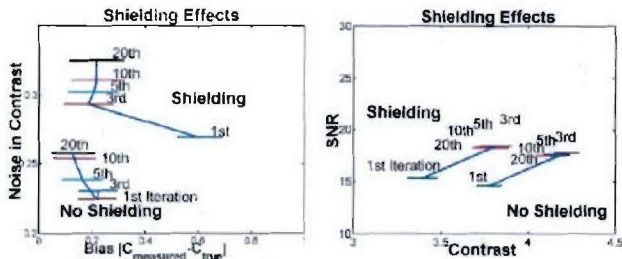| 20th | 3.8±0.1 | 0.32 | 0.2±0.1 | 18.3 |
| 30th | 3.8±0.1 | 0.33 | 0.2±0.1 | 18.3 |

Fig. 6. A) Noise in Contrast vs. Bias.   B) SNR vs. Contrast.

These graphs depict the effect of shielding on the noise in contrast vs. bias and also the SNR v. contrast. Images with lead shielding are more biased and noisier in contrast (A). At a given f_c, contrast is significantly worse with shielding, but SNR is slightly better with shielding than without shielding (B). The horizontal bars represent the standard error (SE)

It is expected that with an OS-EM algorithm, the higher the iteration number, the noisier and the closer to the true contrast the image is. Such characteristics can be roughly observed in both shielded and non-shielded cases. To observe such behavior more clearly, 3-D filtering was applied to the 20th iteration of the reconstructions. The Hann filter, as shown below, was used to smooth these noisy images.

$$H(f) = 0.5*(1+\frac{\cos(\pi f)}{f_c}) \qquad (8)$$

The Hann filter was used with different cutoff (f_c) values and the results are depicted in Table 3. The Noise vs. Bias plot is shown in Fig. 7. Since filtering makes the bias higher and the noise lower, we expected the plot to resemble an inversely proportional curve. The results are mostly consistent with our predictions.

Table 3
Shielding and no shielding table without filtering

Without Shielding - Hann Filter Applied				
cutoff(Vc)	Contrast			SNR
cycles/cm	Mean	Noise	Bias	Mean
1.4	3.6±0.07	0.22	0.5±0.07	24.0
1.6	3.7±0.07	0.23	0.3±0.07	25.0
1.8	3.8±0.08	0.24	0.2±0.08	25.6
2	3.8±0.08	0.25	0.2±0.08	26.1
2.2	3.9±0.08	0.25	0.1±0.08	26.5
2.4	3.9±0.08	0.25	0.1±0.08	26.8
2.6	4±0.08	0.26	0.0±0.08	27.0
With Shielding - Hann Filter Applied				
cutoff(Vc)	Contrast			SNR
cycles/cm	Mean	Noise	Bias	Mean
1.4	3.1±0.08	0.25	0.9±0.08	22.3
1.6	3.3±0.08	0.26	0.7±0.08	23.2
1.8	3.4±0.09	0.27	0.6±0.09	23.9
2	3.4±0.09	0.29	0.6±0.09	24.4

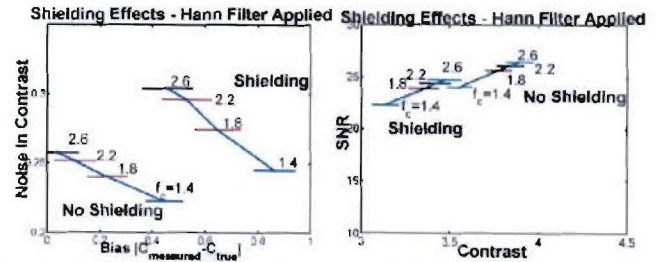| 2.2 | 3.5±0.09 | 0.3 | 0.5±0.09 | 24.7 |
| 2.4 | 3.5±0.09 | 0.3 | 0.5±0.09 | 25.0 |
| 2.6 | 3.5±0.1 | 0.3 | 0.5±0.1 | 25.3 |

Fig. 7. A) Noise in Contrast vs. Bias.   B) SNR vs. Contrast.

The effects of filtering on both noise in contrast and SNR can be seen in these graphs. At a given f_c, images with lead shielding are more biased and noisier in contrast (A). At a given f_c, both SNR and Contrast are better without shielding than with shielding (B).

From both Fig. 6 and Fig. 7, it is clear that shielded images are more biased. A comparison between shielded and non-shielded projection views, shown in Fig. 8, reveals that the non-shielded scans contain a higher number of counts from approximately 180-260 degrees. From the plot it is clear that the lead plate is moderately effective in reducing counts from background scattering.
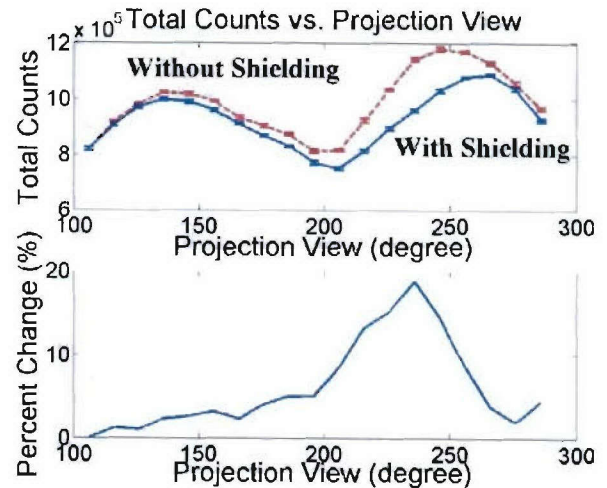
Fig. 8. The upper graph depicts the difference in counts between the shielded images and the unshielded images. It can be seen that the use of shielding moderately decreased the amount of counts by 20%, as depicted in the lower graph.

However, our findings in Fig. 7 are in contradiction with those in Fig. 8. Reduction in background counts (Fig. 8) is expected to decrease bias and increase SNR, but the bias and SNR evaluations prove otherwise. The use of shielding slightly reduced SNR from 26.5 to 24.7 for f_c=2.2 shown Table 3. However, shielding increased the bias in contrast from 0.1+/-0.08 to 0.5+/-0.09. We believe that this obvious

discrepancy may be due to inconsistency in projection data, or to incomplete sampling. As the gamma camera on the triad system rotates around the phantom, significant differences in counts arise when the camera level changes from 'below the lead shielding' to 'above the lead shielding'. With our current reconstruction algorithm, this inconsistency in projection data might have introduced artifacts that lead to undesirable reconstruction results.

IV. CONCLUSION

In this study, we investigated the effects of lead shielding on breast imaging as well as how the radioactive uptake in the myocardium, liver and gall bladder affect the contrast bias and SNR in the phantom breast images. Our results indicate that shielding is moderately effective in reducing the background counts, suggesting potentials to improve lesion detectibility. However, the standard reconstruction algorithms such as OS-EM and ML-EM are limited in reconstructing inconsistent projection data. Comparison of contrast and SNR between shielded and non-shielded images revealed that contrast and SNR is significantly lower with lead shielding than without lead shielding. Although the differences in contrast and SNR are statistically significant, it is difficult to visualize the differences because they were very small.

Future research is required to determine whether and OS-EM algorithm can be implemented that can effectively account for inconsistent projection data.

V. ACKNOWLEDGMENT

VI. REFERENCES

[1] Tornai MP, Bowsher JE, Jaszczak RJ, Pieper BC, Greer KL, Hardenbergh PH, Coleman RE. Mammotomography with pinhole incomplete circular orbit SPECT. Jour. Nuc. Med. 2003; 44(4):594-5.

[2] Scarfone C, Jaszczak RJ, Li J, Soo MS, Smith MF, Greer KL, Coleman RE. Breast Tumor Imaging Using Incomplete Circular Orbit Pinhole SPECT: A phantom study. Nuc. Med. Comm. 1997; 18:1077-1086.

[3] Maublant J, de Latour M, et al. Technetium-99m-Sestamibi Uptake in Breast Tumor and Associated Lymph Nodes. Jour. Nuc. Med. 1996; 37:922-925.

Statistical Analysis of Incomplete Circular Orbits for Breast Pinhole SPECT Imaging

Konstantin V. Bobkov, James E. Bowsher, *Member, IEEE*, Kim L. Greer, Ronald J. Jaszczak, *Fellow, IEEE*, Kelly E. Braun, *Student Member, IEEE*, Tae J. Lee, *Student Member, IEEE*

Abstract-- Breast SPECT imaging with pinhole collimation provides high resolution and sensitivity when the pinhole aperture is in close proximity to the breast. Sampling artifacts can be limited by more nearly satisfying the Tuy complete-sampling requirement. In this study we used clinical count density scans to analyze quantitatively the effects of three acquisition geometries. A Trionix clinical scanner was used with rotation range limited to 180 degrees to simulate the presence of a torso. An isolated breast phantom containing two spherical lesions was mounted on a tiltable platform attached to the patient bed. The orbits were: A) single half-circular orbit (Single HCO), B) three parallel half circles separated axially (Triple parallel HCO), and C) three half circles with the plane of rotation for two half circles tilted +30 and -30 degrees relative to the middle (Triple Tilted HCO). Multiple scans were taken for all orbits to perform statistical analysis. ML-EM was used for reconstruction. Our analysis shows that for the central lesion, orbits B and C yield 31% and 28% higher peak contrast than orbit A. For the side lesion, orbit C gives a 55% higher peak contrast than A and 70% higher than B. Signal-to-noise ratios are dependent on the lesion location. The contrast analysis suggests that triple half-circular orbits are superior to the single half-circular orbit, especially, when two of the circles are tilted so that a larger part of the breast volume stays in the field of view during acquisition.

K. V. Bobkov is with the Department of Radiology, Duke University Medical Center, Durham, NC 27710 USA (telephone: 919-684-7791, e-mail: bobkov@dec3.duhs.duke.edu).

J. E. Bowsher is with the Department of Radiology, Duke University Medical Center, Durham, NC 27710 USA (telephone: 919-684-7788, e-mail: jeb@dec3.duhs.duke.edu).

K. L. Greer is with the Department of Radiology, Duke University Medical Center, Durham, NC 27710 USA (telephone: 919-684-7223, e-mail: klg@dec3.duhs.duke.edu).

R. J. Jaszczak is with the Department of Radiology and the Department of Biomedical Engineering, Duke University Medical Center, Durham, NC 27710 USA (telephone: 919-684-7685, e-mail: rjj@dec3.duhs.duke.edu).

K.E. Braun is a graduate student at Duke University in the Department of Biomedical Engineering, Durham, NC 27710 USA (telephone: 919-684-7784, e-mail: kellyeb@dec3.duhs.duke.edu).

T.J. Lee is a graduate student at Duke University in the Department of Biomedical Engineering, Durham, NC 27710 USA (telephone: 919-684-7784, e-mail: taelee@dec3.duhs.duke.edu).

I. INTRODUCTION

It has been previously suggested that breast SPECT imaging with pinhole collimation may provide an effective tool for characterization of small lesions inside the breast [1-5]. The work of Scarfone et al. [1] with a breast phantom demonstrated the potential to improve visualization of small (< 1 cm) breast tumors. A subsequent patient study with pinhole SPECT [2] revealed a marked improvement in lesion contrast compared to the planar pinhole imaging. The potential advantage of this technique over parallel-beam collimation [6-13,16] is that pinhole can yield high resolution and sensitivity when the pinhole aperture is in close proximity to the breast. Pinhole collimation may also potentially limit scatter contamination from other organs due to the rapid falloff in the sensitivity. At the same time, it is important that the sampled volume stay in the pinhole field of view at every projection to avoid image truncation and that the orbit approximately satisfies the Tuy complete-sampling requirement [14,15]. The sufficient condition for complete sampling of the volume of interest is that the pinhole trajectory must pass through every plane intersecting the volume. When a pinhole collimator is used with the standard clinical scanner, the torso limits the angular range of the camera (Fig. 1) thus making it virtually impossible to sample the entire breast volume completely.
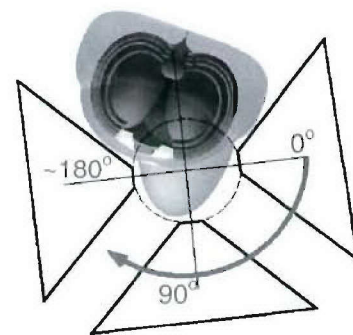

Fig. 1. The figure demonstrates a possible configuration for using a standard clinical scanner with a pinhole collimator to scan a pendulous breast when the patient is in a prone position. The pinhole aperture can be positioned very close to the breast thus increasing resolution and sensitivity. On the other hand, rotation of the camera is limited due to the presence of the torso.

In this work we present three types of acquisition geometries (Fig. 2) for an isolated breast phantom that can completely sample portions of the breast volume to various degrees. However, in this work we did not address the issues such as sampling artifacts and volume distortions due to incomplete sampling. Those studies would ultimately entail doing very high count density scans and/or placing disk phantoms inside the breast [5]. Instead, our primary focus is on clinical count density scans with the phantom containing spherical lesions.
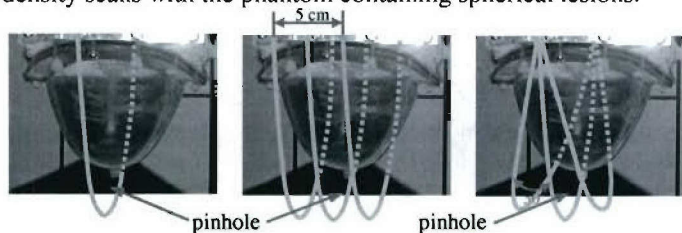

Fig. 2. a) Single HCO   b)Triple Parallel HCO   c) Triple Tilted HCO
       Orbit "A"   Orbit "B"   Orbit "C"
The figure shows three acquisition geometries featured in our study: a) single half circular orbit (Single HCO), b) three parallel half circles separated axially (Triple parallel HCO), and c) three half circles with the plane of rotation for two half circles tilted +30° and -30° relative to the middle circle (Triple Tilted HCO).

The main purpose of this study was to evaluate quantitatively orbits "A", "B", and "C" by calculating contrast and signal-to-noise ratios (SNR) for a statistical ensemble of scans corresponding to each orbit. For this purpose we performed multiple clinical count density scans for each orbit on an isolated breast phantom with lesions and analyzed reconstructed images using statistical methods.

II. METHODS AND MATERIALS

For all scans we used an isolated (volume ~950 mL) breast phantom prototype (~13×15×12 cm^3) with two relatively large spherical ~2.2 cm in diameter (volume ~ 5.5 mL) lesions (Fig. 3) to facilitate region-of-interest (ROI) analysis. The breast bulk was filled with ~3 μCi/mL and the lesions with ~21μCi/mL of ^{99}Tc^m activity yielding a true lesion to background contrast of 6, similar to those currently seen in patients [17].
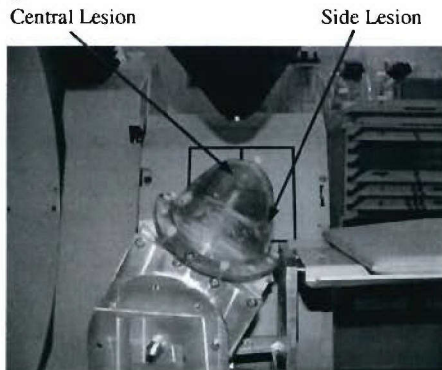

Fig. 3. Figure depicts an isolated breast phantom placed on a tiltable platform attached to the patient bed. Two spherical lesions ~2.2 cm in diameter were placed inside the phantom.

The acquisition times were limited to 135 seconds and combined with the above activity concentrations were approximately equivalent to a clinical scan of 20 minutes. Each scan was corrected for decay to remove the corresponding systematic error from the ensemble. The breast phantom was placed on a custom built tilt platform (Fig. 4a) attached to the translating part of the patient bed and positioned face up. The pinhole collimator (Fig. 4b) had a 20 cm focal length and a 3 mm in diameter knife edge tungsten aperture with an 88° opening angle.

Fig. 4.   a)   b)
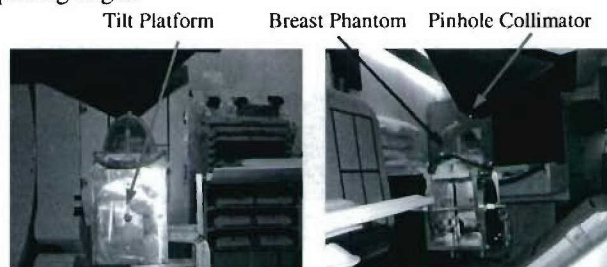a) Custom built tiltable platform that allows the breast phantom to be tilted relative to the plane of rotation of the pinhole in order to acquire a scan corresponding to Triple Tilted HCO (Fig. 2c). b) A different view of the scan setup where the pinhole collimator mounted on the camera can be seen as the breast phantom is scanned.

For all three types of orbits the scanner range was limited to 180° to simulate the presence of a torso. The first orbit (Fig. 2a), previously investigated in [1-2,5], was a half circle with the breast phantom placed on the tilt platform perpendicular to the axis of rotation of the scanner. In a real patient study an uncompressed pendulous breast would be facing down. The radius of rotation (ROR) of the scanner was set to 12.5 cm to ensure that the entire breast phantom always stayed in the field of view (FOV) of the camera during acquisition. This orbit does not require translation of the patient bed and is the easiest to implement with the existing scanners. Its main disadvantage, however, is poor sampling of the breast volume near the chest wall and subsequent volume distortions and incomplete sampling artifacts in reconstructed images. The second orbit (Fig. 2b) consisted of three half circles with parallel planes of rotation, separated axially and perpendicular to the axis of rotation of the scanner [5]. The purpose of having three parallel half circles is to provide a more complete sampling with minimal modifications to the scan setup. This orbit allowed us to reduce the ROR of the pinhole from 12.5 to 10 cm thus increasing the resolution and sensitivity without causing image truncation. In this way, the volume of interest is scanned more evenly which should result in less distorted images and fewer artifacts. The total scan time for this orbit is equal to that of the first orbit, thus resulting in scan time per circle to be three times less. One might naively conclude that the total number of counts in the scan should remain approximately the same as in the first orbit. However, after a closer analysis we can see why that is not the case.

Because the breast has a paraboloid-like shape, the pinhole aperture for the two half circles shifted off the center is effectively further from the volume of interest. Moreover, since the pinhole is shifted sideways its field of view no longer captures the entire breast thus resulting in fewer counts. In order to ameliorate this problem we can modify this acquisition geometry by tilting the pinhole so that its field of view captures the entire breast for all three circles. Therefore, the third orbit (Fig. 2c) featured three half circles with the plane of rotation for the middle half circle perpendicular to the axis along the patient bed and the other two half circles tilted +30° and -30° relative to the plane of rotation of the middle half circle. This was implemented by tilting the platform as depicted in Fig. 3 and readjusting its horizontal and vertical positions. The ROR was again set to 10 cm. In order to produce statistical ensembles we acquired 5 scans for both orbit "A" and "B" and 9 scans for orbit "C".

III. IMAGE RECONSTRUCTION AND ROI ANALYSIS

All images were reconstructed with ML-EM based software. No attenuation or scatter corrections were taken into account in the reconstructions and no post-filtering was performed on the images. The reconstruction grid had pixel dimensions of 128×128×100 with a 2 mm voxel size.
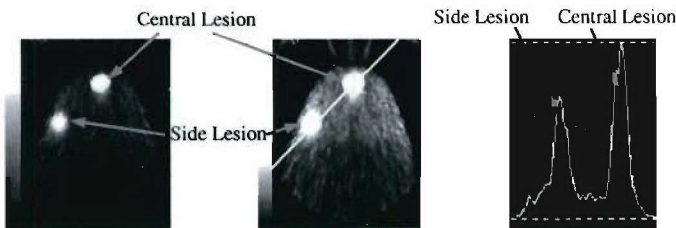

Fig. 5. a) Normal gray scale b) Reduced gray scale c) Oblique profile through the lesion shown in (b). Parts a) and b) feature a sagittal slice of a typical reconstructed image for orbit "B" (Fig. 2b) after 5 iterations in which both lesions are clearly visible.

Reconstructions for orbits "A" and "C" are qualitatively similar. As can be seen from the profile (Fig. 5c), the central lesion has a markedly higher peak in comparison with the side lesion. This is reflected quantitatively in our subsequent ROI analysis. It was expected given the acquisition geometry because the pinhole aperture was closer to the central lesion during acquisition. The apparent gradient in the bulk activity can be attributed to attenuation and scatter. This may pose a potential problem in defining a background ROI. However, we were able to circumvent this problem by choosing spherical-shell "Background ROIs" (Fig. 6b) surrounding the lesions. Spherical "Lesion ROIs" (Fig. 6c), centered at the centroids of both lesions, were chosen to be 2.2 cm in diameter which is equal to the physical diameter of the lesions used in the experiments. For every orbit, our ROI analysis included image frames for iterations 1-5, 10, 15, 20, and 25. Let us consider an example for orbit "C" where we took 9 scans in order to clarify what we mean by a statistical ensemble. In this case a single

ensemble consists of nine reconstructed images (because we took nine scans) taken after the same number of iterations. Thus for every iteration 1-5, 10, 15, 20, and 25 we have an ensemble of 9 images.
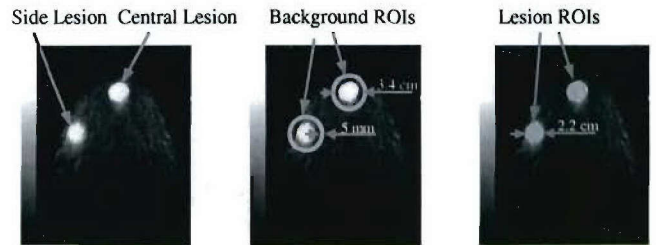

Fig. 6. a) Sagittal slice   b) Background ROIs   c) Lesion ROIs
Figure a) shows a sagittal slice of a reconstruction for orbit "B" after 5 ML-EM iterations. Figure b) shows the same slice as in a) with two spherical-shell "Background ROIs". Figure c) shows the same sagittal slice with two spherical "Lesion ROIs".

For both lesions we found mean activity in the lesion and the background and calculated corresponding standard deviations and standard errors of the mean.

For a given statistical ensemble of scans corresponding to the same iteration frame, mean activity was defined by

$$\overline{N} = \frac{1}{n}\sum_{i=1}^{n} N_i , \qquad (1)$$

where N_i are the total number of counts inside an ROI for the i-th scan and $n=9$ for orbit "C" and $n=5$ for orbits "A" and "B". Standard deviation for an ensemble was defined as

$$\sigma_N = \sqrt{\frac{\sum_{i=1}^{n}\left(\overline{N} - N_i\right)^2}{n-1}} . \qquad (2)$$

Standard error of the mean:

$$\overline{\sigma}_N = \frac{\sigma_N}{\sqrt{n}} . \qquad (3)$$

We then determined contrasts and SNRs by applying the following definitions:

$$Contrast = \frac{\left|\overline{N}_{lesion} - \overline{N}_{bg}\right|}{\overline{N}_{bg}} \qquad (4)$$

$$SNR = \frac{\left|\overline{N}_{lesion} - \overline{N}_{bg}\right|}{\sigma_{N_{bg}}} . \qquad (5)$$

The uncertainty in contrast was determined by using standard propagation of error techniques. This analysis was performed on both lesions for all three orbits with the results presented in the next section.

IV. RESULTS

We divided our results into two sets corresponding to the two lesions – central lesion and side lesion. Tables 1, 4

correspond to single half circular orbit (Single HCO) (Fig. 2a), Tables 2, 5 to triple parallel HCO (Fig. 2b) and Tables 3, 6 to triple tilted HCO (Fig. 2c). Each table shows how values of contrast and SNR change when going from low to high iterations. Recall that the true contrast value determined by the lesion and bulk activities used in the experiment was 6. As expected from ML-EM reconstruction algorithms, when we follow the change in contrast from iteration to iteration, we notice that after a rapid increase during low iterations, for iterations 10 and higher, contrast value for a particular orbit stays approximately the same within the margin of uncertainty. Signal-to-noise ratios do not display such a clear trend. However, most peak SNR values occurred between iterations 5 and 10 (Table 1 is the only exception). Overall, the SNR values are quite large. This feature can be attributed to vary small deviations of the total number of counts N_i in the i-th spherical shell "Background ROI" from the mean value in an ensemble resulting in small σ_{Nbg} and large SNR. This is a direct consequence of the definition of the standard deviation σ_{bg} in equation (2).

A. Central Lesion

Tables 1-3 contain contrast and SNR values for the central lesion located closer to the nipple. The values in bold indicate peak contrast and SNR.

Table 1. (Orbit "A" – Single Half Circle)

Iteration	1	5	10	15	20	25
Contrast	0.70±0.01	3.69±0.02	4.41±0.02	4.47±0.02	4.53±0.02	**4.55±0.03**
SNR	44.72	305.41	409.41	550.6	**556.8**	354.18

Table 2. (Orbit "B"- Three Parallel Half Circles)

Iteration	1	5	10	15	20	25
Contrast	0.70±0.02	4.48±0.03	5.89±0.03	**5.96±0.05**	5.86±0.04	5.89±0.04
SNR	32.65	148.25	**226.62**	174.53	176.64	177.52

Table 3. (Orbit "C"- Three Tilted Half Circles)

Iteration	1	5	10	15	20	25
Contrast	0.66±0.01	4.30±0.06	5.68±0.07	5.80±0.08	**5.81±0.08**	5.80±0.08
SNR	3.74	**275.16**	243.72	194.45	180.07	164.18

If we compare peak contrast values from Tables 1-3, orbits "B" and "C" yield 31% and 28% higher contrast than orbit "A". On the other hand, peak SNR values give a clear advantage to orbit "A" which is expected since the central lesion always stays in the field of view for this orbit. In addition to that, the pinhole aperture stays close to the central lesion for a longer duration of time for orbit "A" since the total scan times are kept the same for all orbits. In other words, the single half circle of orbit

"A" will yield more counts and therefore higher SNR for the central lesion.

B. Side Lesion

Tables 4-6 contain contrast and SNR values for the side lesion located near the chest wall.

Table 4. (Orbit "A" – Single Half Circle)

Iteration	1	5	10	15	20	25
Contrast	0.50±0.01	1.76±0.03	2.28±0.04	2.44±0.03	2.51±0.04	**2.52±0.04**
SNR	32.51	**107.45**	103.02	104.76	90.8	88.66

Table 5. (Orbit "B"- Three Parallel Half Circles)

Iteration	1	5	10	15	20	25
Contrast	0.48±0.01	1.84±0.04	2.20±0.05	2.26±0.05	2.28±0.06	**2.30±0.06**
SNR	16.43	115.75	**150.81**	102.07	95.93	96.6

Table 6. (Orbit "C"- Three Tilted Half Circles)

Iteration	1	5	10	15	20	25
Contrast	0.44±0.01	2.29±0.02	3.32±0.04	3.67±0.06	3.81±0.08	**3.91±0.07**
SNR	27.33	93.97	**110.87**	102.8	83.51	95.5

The location of the side lesion clearly makes it less biased in favor of any particular orbit under consideration. The impact of location on contrast recovery and SNR is seen immediately once we compare the peak values in Tables 4-6 with those in Tables 1-3. This difference points to the difficulty with all three orbits of visualizing lesions located deep inside the breast near the chest wall. Nevertheless, when we compare peak contrast values from Tables 4-6, orbit "C" gives a 55% higher contrast than orbit "A" and 70% higher than orbit "B". Peak SNR values give a slight advantage to orbit "B".

V. DISCUSSION

Three types of orbits that can be used for breast SPECT imaging using pinhole collimation have been investigated. The single half circular orbit (Orbit "A", Fig. 2a) can be easily implemented on a standard clinical scanner. However, the necessity to keep the entire breast in the field of view of the camera to avoid truncation forces us to increase the radius of rotation of the camera resulting in the loss of sensitivity and resolution. Moreover, the single HCO yields very uneven sampling with the most complete sampling being in the slice corresponding to the plane of rotation of the pinhole. Multiple half circular orbits provide for a possibility to decrease the ROR and improve sampling of the peripheral parts of breast. Orbit "B" (Fig. 2b), featuring three parallel half circles can also be implemented on a standard scanner by combining rotation of the scanner with translation of the patient bed. The main disadvantage of this orbit, however, is that during a significant

part of an acquisition scan the breast is no longer entirely in the field of view of the camera. This happens when the pinhole is axially shifted and part of the breast is truncated. The most obvious solution to this problem was to tilt the planes of rotation of the two circles that are off center so that the entire breast stays in the field of view during acquisition. Thus, orbit "C" (Fig. 2c) had two of the half circles tilted relative to the plane of rotation of the middle circle.

We used an isolated breast phantom with two relatively large lesions and took multiple clinical count density scans for each orbit type. The total scan times were the same for all orbits and decay correction was accounted for. All images were reconstructed with ML-EM. Attenuation and scatter corrections were not taken into account in the reconstructions. Spherical "Lesion ROIs" and spherical-shell "Background ROIs" were defined surrounding the lesions in order to find contrast and signal-to-noise ratios in the reconstructed images. Each iteration of ML-EM provided a statistical ensemble of reconstructed images for each orbit obtained from a set of multiple scans. For every ensemble of images taken after iterations 1-5, 10, 15, and 20 we determined mean contrast and SNR and assembled all the values into Tables 1-6. From the peak contrast values we discovered that for the central lesion orbits "B" and "C" were superior in contrast recovery compared to orbit "A". For the side lesion located near the chest wall, orbit "C" yielded the best contrast recovery. Peak SNR values for the central lesion gave a clear advantage to orbit "A" which can be attributed to the bias in the central lesion location. For the side lesion, however, peak SNR values indicated that orbit "B" has a slight advantage.

VI. CONCLUSIONS

Our results suggest that triple half circular orbits are superior to the single half circular orbit, especially when two of the circles are tilted so that a larger part of the breast volume stays in the field of view during acquisition. In this investigation we did not take into account attenuation and scatter corrections which will change total counts in the ROIs. We leave this for a future study. Nevertheless, our choice of "Background ROIs" partially compensated for this error. Single HCO and triple HCO can be readily implemented on a standard clinical scanner, whereas the triple tilted HCO would require building a dedicated system.

VII. REFERENCES

[1] C. Scarfone, R.J. Jaszczak, J. Li, M.S. Soo, M.F. Smith, K.L. Greer, and R.E. Coleman. Breast tumour imaging using incomplete circular orbit pinhole SPET: A phantom study. Nucl. Med. Comm., 1997, 18, 1077-1086.

[2] M.P. Tornai, J.E. Bowsher, R.J. Jaszczak, B.C. Pieper, K.L. Greer, P.H. Hardenbergh, and R.E. Coleman. Mammotomography with Pinhole Incomplete Circular Orbit SPECT. J Nucl Med 2003 44:583-593.

[3] Seret A, Defrise M, Blocket D. 180-degree pinhole SPET with a tilted detector and OS-EM reconstruction: phantom studies and potential clinical applications. Eur J Nucl Med. 2001; 28:1836-1841.

[4] JE Bowsher, MP Tornai, SD Metzler, J Peter, RJ Jaszczak: "SPECT breast imaging using more nearly complete orbits and combined pinhole-parallel-beam collimation", Conf Rec 2001 NSS/MIC.

[5] KV Bobkov, JE Bowsher, SD Metzler, KL Greer, RJ Jaszczak: "Multicircular, helical, and x-type orbits for SPECT pinhole breast imaging", J Nucl Med (2004) 45:157P.

[6] H Wang, C Scarfone, KL Greer, RE Coleman, RJ Jaszczak: "Prone breast tumor imaging using vertical axis-of-rotation VAOR SPECT systems: An initial study", Trans Nucl Sci (1997) 44:1271-1276.

[7] BC Pieper, JE Bowsher, MP Tornai, J Peter, KL Greer, RJ Jaszczak: "Breast tumor imaging using a tiltable head SPECT camera", Trans Nucl Sci (2001) 48:1477-1482.

[8] Tornai MP, Bowsher JE, Archer CN, et al. Dedicated breast imaging with an ASET: application specific emission tomography. J Nucl Med. 2001; 42 (suppl): 97P.

[9] Tornai MP, Bowsher JE, Archer CN, et al. A novel application specific emission tomography (ASET) for breast imaging. 2001 IEEE Med Imaging Conf Rec. 2001; 2:1161-1165.

[10] SD Metzler, JE Bowsher, MP Tornai, BC Pieper, J Peter, RJ Jaszczak: "SPECT breast imaging combining horizontal and vertical axes of rotation", Trans Nucl Sci (2002) 49:31-36.

[11] CN Archer, MP Tornai, JE Bowsher, SD Metzler, BC Pieper, RJ Jaszczak: "Implementation and initial characterization of acquisition orbits with a dedicated emission mammotomograph", Trans Nucl Sci (2003) 50:413-420.

[12] MP Tornai, JE Bowsher, CN Archer, J Peter, RJ Jaszczak, LR MacDonald, BE Patt, JS Iwanczyk: "A 3D gantry single photon emission tomograph with hemispherical coverage for dedicated breast imaging", Nucl Inst Meth Phys Res A (2003) 497:157-167.

[13] W.H. Baird, EC Frey, BMW Tsui, YC Wang, and DE Wessell. Evaluation of rotating slant-hole SPECT mammography using Monte Carlo simulation methods. IEEE Transactions on Nuclear Science, 50:105-109, 2003.

[14] Heang K. Tuy. An Inversion Formula for Cone Beam Reconstruction. SIAM J. Appl Math. (1983) Vol. 43:546-552.

[15] SD Metzler, JE Bowsher, RJ Jaszczak: "Geometrical Similarities of the Orlov and Tuy Sampling Criteria and a Numerical Algorithm for Assessing Sampling Completeness", Trans Nucl Sci (2003) 50:1550-1555.

[16] RL McKinley, MP Tornai, E Samei, ML Bradshaw: "Simulation study of a quasi monochromatic beam for x-ray computed mammotomography", Med Phys (2004) 31:800-813.

[17] Maublant J, de Latour M, Mestas D, Clemenson A, Charrier S, Feillel V, Le Bouedec G, Kaufmann P, Dauplat J, Veyre A. Technetium-99m-sestamibi uptake in breast tumor and associated lymph nodes. J Nucl Med. 1996 Jun;37(6):922-925.

Reduced Incomplete-Sampling Artifacts in Pinhole SPECT Breast Imaging Using Body-Contour and Lung-Boundary Constraints

James E. Bowsher, *Member, IEEE,* Tae Lee, *Member, IEEE,* Kelly Braun, *Member, IEEE,*
Konstantin V. Bobkov, *Member, IEEE,* and Ronald J. Jaszczak, *Fellow, IEEE*

Abstract—Dedicated systems for SPECT breast imaging offer improved spatial resolution and sensitivity by maintaining close proximity to the breast throughout the gamma camera orbit. However, generally these systems do not adequately sample the important regions of the breast-torso interface and the axilla. Herein we consider the potential of body-contour and lung-boundary information for reducing incomplete-sampling artifacts in these regions. Given the increasing predominance of multi-modality imaging, such information might be available from CT, MRI, or optical imaging. The studies presented here show that such information can significantly improve estimates of radiotracer activity in and near tumors. The studies also suggest that such information may be able to improve detection of focal hot spots.

Index Terms— SPECT, breast cancer, CT, MRI, optical imaging

I. INTRODUCTION

Dedicated SPECT systems have been developed for imaging the breast [1]–[14]. A general notion of these systems is to orbit about the breast specifically rather than about the torso generally. Hence parallel-beam, vertical axis of rotation (VAOR) breast imaging has been proposed [1], in which the patient lies prone and a gamma camera orbits about the suspended breast, with the axis of rotation being a vertical line from the torso to the nipple. Such orbits avoid acquisition through the attenuating patient torso, and they improve spatial resolution by allowing the SPECT gamma camera to be close to the breast [1], [3]. Ideal observer studies have shown a consequent substantial improvement in signal-to-noise ratio (SNR) for dedicated parallel-beam SPECT imaging, as compared to orbiting the entire torso [3]. Even greater proximity can be obtained by tilting the gamma camera, and tilting also increases projection sampling of activity near the breast-torso interface [4]. However, such orbits create distortions because tilted circular orbits of parallel-beam collimators do not satisfy Orlov's sampling criteria [4]. Accordingly, orbits have been proposed which satisfy Orlov's condition for a limited region of space (assuming untruncated

projections) [4], [7]–[9]. For example, the advantages of the parallel-beam tilted-circular orbit might be retained while also providing more nearly complete sampling by adding an arc to the orbit [4], [7]–[9]. A dedicated breast imaging hardware acquisition system has been developed [8], [9], and it has demonstrated experimentally the ability to orbit closely about the breast, acquiring high resolution parallel-beam data, while also avoiding incomplete-sampling artifacts throughout much of breast [8], [9]. However, the region for which complete sampling can be obtained, while maintaining close proximity to the breast throughout the orbit, is limited. This completely sampled volume tends not to extend into the breast torso interface or into the important axilla region, and consequently the estimated radiotracer distribution in these important regions can be highly distorted.

Dedicated pinhole SPECT breast imaging has also been proposed, again with the notion of orbiting about the breast specifically rather than the torso generally [2], [5], [6], [11], [12], [14]. Pinhole collimation offers the potential of high spatial resolution and high sensitivity in portions of the breast that are near the pinhole throughout much of the gamma camera orbit. Because the larger gamma camera is displaced from the pinhole by the pinhole focal length, both VAOR and horizontal-axis-of-rotation (HAOR) orbits are possible while maintaining close proximity of the pinhole to the breast. An important characteristic of HAOR pinhole orbits is that they can be implemented on existing standard SPECT scanners with the patient prone. Partial-circle pinhole orbits about the breast have been proposed and investigated in [2], [11]. Partial-circle orbits, in which the pinhole remains within a single plane, provide a completely sampled volume for only a portion of that plane. Accordingly, 3-dimensional HAOR pinhole orbits have been proposed which provide a completely sampled 3D volume (under Tuy's condition assuming that projections are not truncated) [6]. These orbits can be implemented by combining standard HAOR SPECT gantry motion with translation of the patient bed. VAOR pinhole orbits are also being investigated [12], which would involve either the patient sitting up next to a standard SPECT gantry or the patient laying prone over a dedicated gantry. The study [12] also suggested that 3-dimensional yet incompletely-sampling orbits, such as two offset circles, may provide acceptably low incomplete-sampling artifacts in the vicinity of the circles, particularly given the

greater simplicity with which such orbits can be implemented. All these studies show promise for pinhole SPECT breast imaging near the nipple and extending substantially into the mid-breast region. However, as with parallel-beam imaging, they also generally show increasing distortions, at some point, approaching the breast-torso interface and the axilla [2], [6], [11], [12].

Hence, the development of dedicated breast imaging systems is progressing, and their potential is becoming increasingly clear. Yet, it is apparent that these methods typically result in artifacts near the breast-torso interface and in the axilla, regions which are important for diagnosis of breast cancer. One approach to addressing incomplete sampling of these regions is to augment the dedicated breast imaging scans with some form of full-torso SPECT scan, as has been suggested for pinhole [6] and parallel-beam [7] breast scans. Another form of additional information about radiotracer distribution is in the outer contours of the patient and in patient lung boundaries. Patient contours can be obtained by optical imaging. Both patient contours and lung-boundaries can be obtained by high-resolution CT, by lower-resolution transmission tomography using radio-isotope sources, and by MRI. When these other imaging modalities are employed anyway, for the diagnostic information they provide, there may be particularly good cost-benefit trade-offs in also utilizing this information to improve estimation of the radiotracer distribution. Many of the dedicated parallel-beam and pinhole SPECT breast imaging systems, particularly the VAOR systems, are designed to be small and portable, raising the possibility that these systems might be rolled up to the patient bed for an inherently registered SPECT scan following a CT scan. Also, a dedicated VAOR breast CT/SPECT system is being developed [13]. The advent of general-purpose HAOR CT/SPECT systems raises the possibility of inherently registered CT and HAOR pinhole SPECT scans of the breast. Herein, we utilize computer-simulation studies to investigate the potential of such patient-contour and lung-boundary information for improving the estimation of SPECT radiotracer distribution.

II. METHODS

Computer-simulated three-dimensional phantom distributions of radiotracer and attenuation were generated for the heart, two lungs, the torso, one breast, and 15 spherical hot spots. The phantom was constructed using ellipsoids, as shown in Fig. 1, and was then implemented on a grid of 0.1-cm-wide voxels. For example, the breast was comprised of all 0.1-cm-wide voxels such that the voxel center was within the breast ellipsoid yet outside the torso, lung, heart, and hot-spot ellipsoids. The radii of the breast ellipsoid were 8 cm in the x and y directions and 16 cm in the axial, z direction. Fig. 1 illustrates a patient in prone position, with the breast suspended and the z-axis vertical, directed from the chest to the nipple. Ellipsoids for the spherical hot spots were 0.5 cm in radius. Radii for the lungs, heart, and torso ellipsoids were (r_x, r_y, r_z) = (9 cm, 12 cm, 10 cm), (5.5 cm, 5.5 cm, 7 cm), and (22 cm,
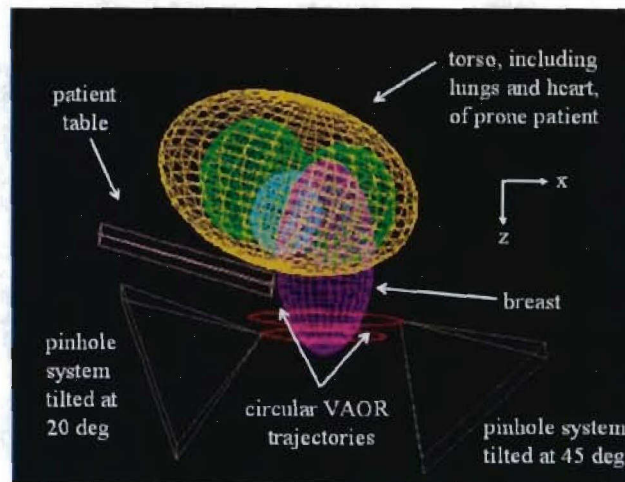

Fig. 1. Phantom and Orbits

50 cm, 14 cm), respectively. Relative radiotracer activities in tumor:heart:torso:lung were 6:3:1:0. The radiotracer phantom from which projection data were simulated was then obtained by summing $2 \times 2 \times 2$ cubes of 0.1-cm-wide voxels into 0.2-cm-wide voxels. Phantom attenuation was 0.15 per cm, except in the lungs where it was 0.05 per cm.

The orbit of the pinhole-collimated gamma camera is also illustrated by Fig. 1. This orbit involves two circular trajectories of the pinhole, with the plane of each trajectory being perpendicular to the z axis. In order to allow greater proximity of the pinhole and gamma camera to the breast and torso, the pinhole and gamma camera are tilted relative to the z axis by 45 degrees for the inner circle (the circle closer to the torso and at lower z) and by 20 degrees for the outer circle. (Tilted pinhole is also investigated in [15].) A two-offset-circles pinhole trajectory does not satisfy Tuy's sufficient sampling condition for any three-dimensional volume. However, such orbits warrant investigation because of the simplicity with which they can be implemented, and in practice, these orbits can provide reconstructed images with relatively little distortion between and near the planes of the circles [12]. Tilting the pinholes may further degrade sampling for the outer portions of the breast, but it allows greater proximity to the breast, and it increases sampling of the breast-torso interface and the axilla, regions which are important for breast cancer imaging. Noise-free projection data were computer-simulated for 512×256 0.089-cm-wide projection bins at each of 128 pinhole locations evenly spaced over each of the two circles. For each detector bin, the computer simulation utilized an inverse cone [16] of nine rays in order to model a knife-edge pinhole 0.3 cm in diameter. The pinhole opening angle was 88 degrees, and the pinhole was located 20 cm from the detector image plane. In order to model detector crystal resolution, these ray-tracing results were blurred with a 0.35-cm full-width-at-half-maximum Gaussian kernel. Psuedo-random sampling was then employed to generate noisy Poisson-distributed data with 4-

and 1-million total measured events.

For the noise-free data and each of the two noisy data sets, three reconstructions were performed: (i) Activity was estimated over a support extending throughout the phantom and well past the phantom body contours. (ii) Support was restricted to within body contours. (iii) Support was restricted to within body contours and outside the lungs. The support restriction (ii) incorporates into image reconstruction the knowledge that activity is zero outside of the phantom body. The support restriction (iii) incorporates the knowledge that activity is zero outside the phantom body and within the phantom lungs. For all reconstructions there were 5 iterations of OSEM [17] with 16 subsets. The reconstructions modeled spatially varying attenuation but did not model pinhole size or detector crystal resolution. A Hanning filter was applied to reconstructions from the noisy data sets. Filter cutoffs were $0.8F_n$ (4-million-count data) and $0.6F_n$ (1-million-count data), where the Nyquist frequency F_n was 2.5 cycles per cm.

III. RESULTS

A two-offsets-circles VAOR pinhole trajectory [12] may have practical advantages in terms of its ease and relatively low cost of implementation. Although this trajectory does not strictly satisfy Tuy's condition for any three-dimensional volume, profile #2 in Fig. 2 suggests that the orbit provides information sufficient to obtain a good reconstruction of the outer portion of the breast. All three reconstructions, including the one which relies solely on SPECT projection data (Fig. 2d), accurately recover the flat shape of the breast background activity. More sophisticated orbits might sample an even greater portion of the mid and outer breast [6], [12], [14]. However, even with many of those orbits, sampling is inadequate in the axilla and near the breast torso interface. Profile #1 and the associated arrows identify a background region in the axilla which is highly distorted when image reconstruction uses only the SPECT projection data (Fig. 2d). The estimate is significantly improved by the use of body-contour information (Fig. 2c). The combined use of body-contour and lung-boundary information results in a quite accurate estimate of background activity in the axilla (Fig. 2b).

Profile #1 of Fig. 3 indicates that, in the absence of lung-boundary information (Fig. 3d and 3c), the reconstructed radiotracer distribution shows the lung extending too far toward the breast. The use of lung-boundary and body-contour information (Fig. 3b) provides an improved estimate of radiotracer distribution in this region. Body-contour information alone did not improve the reconstruction in this region. Profile #2 shows that in the mid-breast region, use of both body-contour and lung-boundary information (Fig. 3b) provides a reconstructed image which, to within random noise variations, reproduces the flat shape of the phantom background distribution. Both types of information are beneficial: The reconstruction of Fig. 3c using body-contour information only is more accurate than Fig. 3d but less accurate than Fig. 3b.

In Fig. 4, the arrows for profile #1 identify a region of the axilla in which background activity is greatly underestimated
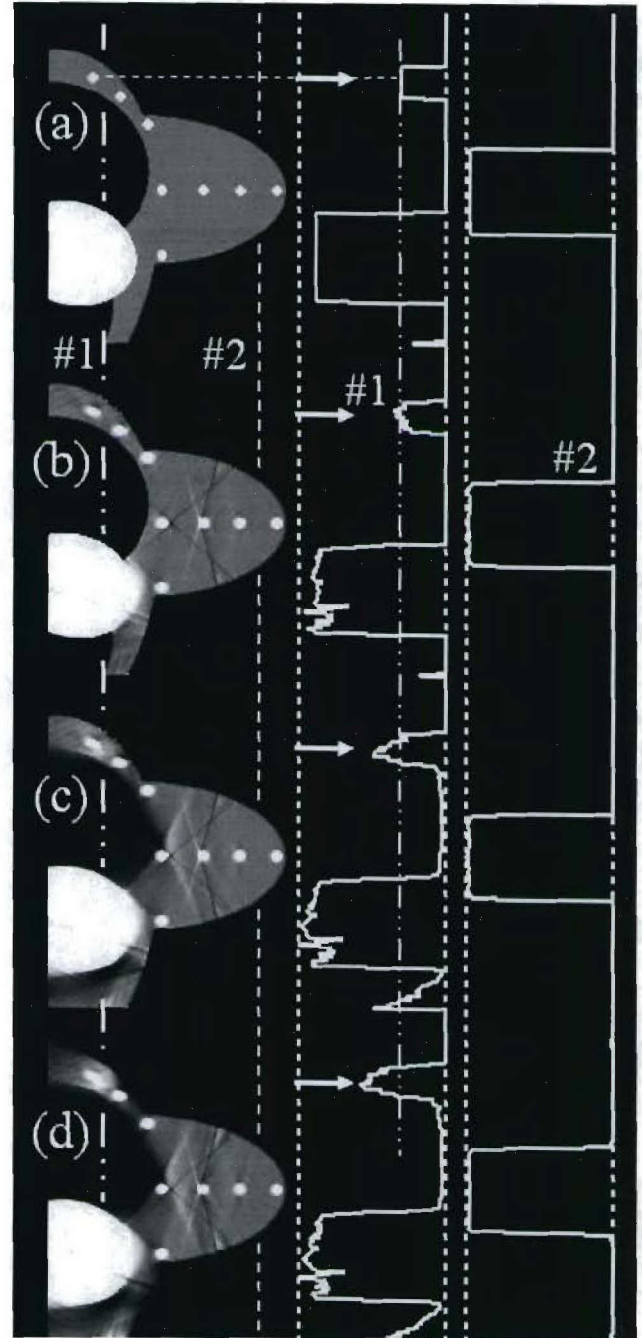

Fig. 2. Noise-free study. (a) Phantom. (b-d) Reconstruction from noise-free projection data using body-contour and lung-boundary information (b), body-contour information only (c), no body-contour or lung-boundary information (d). Lines #1 and #2 through the images indicate locations of corresponding profiles. Arrows indicate the same locations along the profiles through different images. The dash-dot line through profile #1 indicates the phantom activity in the region of interest.
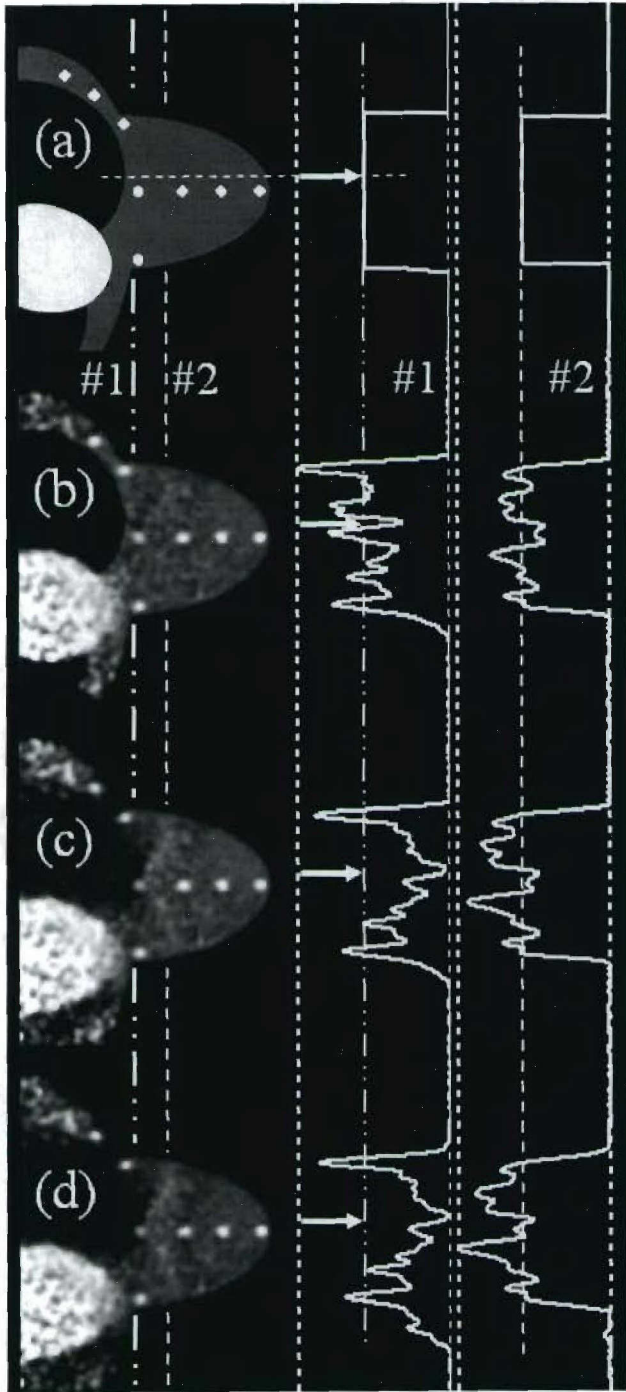
Fig. 3. Four-million-count study. (a) Phantom. (b-d) Reconstruction from 4-million count projection data using body-contour and lung-boundary information (b), body-contour information only (c), no body-contour or lung-boundary information (d). Lines #1 and #2 through the images indicate locations of corresponding profiles. Arrows indicate the same locations along the profiles through different images.

in the image reconstructed from SPECT projection data only (Fig. 4d). The estimate of background activity is improved by the use of body-contour information (Fig. 4c), and is fairly accurate when body-contour and lung-boundary information are utilized (Fig. 4b). The arrows for profile #2 in Fig. 4 locate the center of the lesion near the breast-torso interface. The estimated amplitude of the lesion is significantly higher when body-contour and lung-boundary information are utilized (Fig. 4b). Use of body-contour information alone (Fig. 4c) does not signficantly improve upon estimation from the SPECT projection data only (Fig. 4d). Looking at the images, there are numerous spurious structures in Fig. 4d and 4c with sizes and contrasts comparable to that estimated for the lesion. Hence the signal-to-noise ratio (SNR) of the lesion in Fig. 4d and 4c is too low for detection in the absence of knowledge such as lesion location. Lesion SNR is higher in Fig. 4b. Although detectability cannot be fully assessed from a single noisy realization, these results suggest the possibility that use of body-contour and lung-boundary information may have the potential to improve lesion detection in the vicinity of the breast-torso interface.

IV. CONCLUSIONS AND DISCUSSION

Figures 2-4 all show considerable distortions in the estimated background activity when activity is estimated from SPECT projection data alone. Left uncorrected, these distortions could be detrimental in several ways, including: (i) The distortions can alter tumor-to-background uptake ratios, giving spuriously low or high results, and thus potentially undermining the clinical use of such ratios. (ii) The distortions may undermine the use of SPECT images for guiding biopsy, since the distortions create uncertainty about the locations of landmarks, such as the body contour and the lung boundaries. (iii) Biochemistry in the vicinity of the tumor is becoming increasingly important in understanding and treating cancer, and distortions in estimated activity about a focal spot of tumor undermine the imaging of this biochemistry. The results presented here show a marked reduction in these distortions through the use of body-contour and lung-boundary information. With regard to imaging focal spots of high radiotracer uptake, the 1-million-count study suggests that it may be possible to improve detection through the use of body-contour and lung-boundary information.

This study considers crisp lung boundaries with known activity of zero. An important extension is to include the use of motion-blurred lung boundaries and the estimation of small but spatially varying lung activity. This study emphasizes reducing incomplete-sampling artifacts by incorporating the boundaries of large-scale anatomical structures — body contours and lung boundaries. There may also be significant benefit from incorporating smaller scale structure, e.g. from MRI and CT, in order to alleviate the degrading effects of SPECT noise and limited SPECT spatial resolution.

REFERENCES

[1] H. Wang, C. Scarfone, K.L. Greer, R.E. Coleman, and R.J. Jaszczak. Prone breast tumor imaging using vertical axis-of-rotation (VAOR)
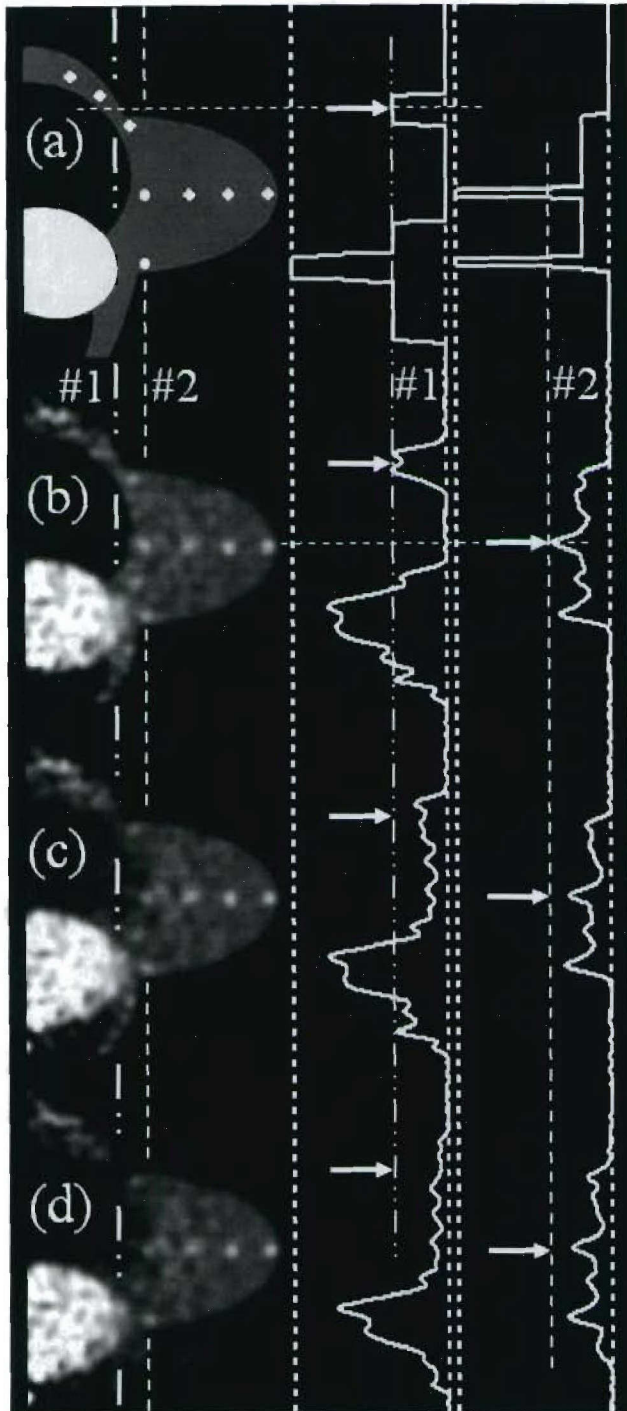
Fig. 4. One-million-count study. (a) Phantom. (b-d) Reconstruction from 1-million count projection data using body-contour and lung-boundary information (b), body-contour information only (c), no body-contour or lung-boundary information (d). Lines #1 and #2 through the images indicate locations of corresponding profiles. Arrows indicate the same locations along the profiles through different images.

SPECT systems: An initial study. *IEEE Trans Nucl Sci*, 44:1271–1276, 1997.

[2] C. Scarfone, R.J. Jaszczak, J. Li, M.S. Soo, M.F. Smith, K.L. Greer, and R.E. Coleman. Breast tumor imaging using incomplete orbit pinhole SPET: a phantom study. *Nucl Med Commun*, 18:1077–1086, 1997.

[3] P.J. La Riviere, X. Pan, and B.C. Penney. Ideal observer analysis of lesion detectability in planar, conventional SPECT, and dedicated SPECT scintimammography using effective multi-dimensional smoothing. *IEEE Trans Nucl Sci*, 45:1273–1279, 1998.

[4] B.C. Pieper, J.E. Bowsher, M.P. Tornai, J. Peter, K. Greer, and R.J. Jaszczak. Breast tumor imaging using a tiltable head SPECT camera. *IEEE Transactions on Nuclear Science*, 48:1477–1482, 2001.

[5] F.H. Fahey, K.L. Grow, R.L. Webber, B.A. Harkness, E. Bayram, and P.F. Hemler. Emission tuned-aperture computed tomography: A novel approach to scintimammography. *Journal of Nuclear Medicine*, 42:1121–1127, 2001.

[6] J.E. Bowsher, M.P. Tornai, S.D. Metzler, J. Peter, and R.J. Jaszczak. SPECT breast imaging using more nearly complete orbits and combined pinhole-parallel-beam collimation. In *Conference Record of the 2001 IEEE Nuclear Science Symposium and Medical Imaging Conference*.

[7] S.D. Metzler, J.E. Bowsher, M.P. Tornai, B.C. Pieper, J. Peter, and R.J. Jaszczak. SPECT breast imaging combining horizontal and vertical axes of rotation. *IEEE Transactions on Nuclear Science*, 49:31–36, 2002.

[8] C.N. Archer, M.P. Tornai, J.E. Bowsher, S.D. Metzler, B.C. Pieper, and R.J. Jaszczak. Implementation and initial characterization of acquisition orbits with a dedicated emission mammotomograph. *IEEE Transactions on Nuclear Science*, 50:413–420, 2003.

[9] M.P. Tornai, J.E. Bowsher, C.N. Archer, J. Peter, R.J. Jaszczak, L.R. MacDonald, B.E. Patt, and J.S. Iwanczyk. A 3D gantry single photon emission tomograph with hemispherical coverage for dedicated breast imaging. *Nuclear Instruments and Methods in Physics Research A*, 497(1):157–167, 2003.

[10] W.H. Baird, EC Frey, BMW Tsui, YC Wang, and DE Wessell. Evaluation of rotating slant-hole SPECT mammography using Monte Carlo simulation methods. *IEEE Transactions on Nuclear Science*, 50:105–109, 2003.

[11] M.P. Tornai, J.E. Bowsher, R.J. Jaszczak, B.C. Pieper, K.L. Greer, P.H. Hardenbergh, and R.E. Coleman. Mammotomography with pinhole incomplete circular orbit SPECT *Journal of Nuclear Medicine*, 44:583–593, 2003.

[12] K.V. Bobkov, J. E. Bowsher, S.D. Metzler, K.L. Greer, and R.J. Jaszczak. Multicircular, helical, and x-type orbits for SPECT pinhole breast imaging. *Journal of Nuclear Medicine*, 45:157P (abstract), 2004.

[13] R.L. McKinley, M.P. Tornai, E. Samei, and M.L. Bradshaw. Simulation study of a quasi monochromatic beam for x-ray computed mammotomography. *Med Phys*, 31(4):800–813, 2004.

[14] K.V. Bobkov, J. E. Bowsher, R.J. Jaszczak, and K.L. Greer. Statistical analysis of incomplete circular orbits for breast pinhole SPECT imaging. In *Conference Record of the 2004 IEEE Nuclear Science Symposium and Medical Imaging Conference*, Rome, Italy, October 16-24 2004.

[15] A. Seret, M. Defrise, and D. Blocklet. 180 pinhole SPET with a tilted detector and OS-EM reconstruction: Phantom studies and potential clinical applications. *Eur J Nucl Med*, 28:1836–1841, 2001.

[16] B.M.W. Tsui, H.B. Hu, D.R. Gillland, and G.T. Gullberg. Implementation of simultaneous attenuation and detector response correction in SPECT. *IEEE Transactions on Nuclear Science*, 35:778–783, 1988.

[17] H.M. Hudson and R.S. Larkin. Accelerated image reconstruction using ordered subsets of projection data. *IEEE Trans Medical Imaging*, 13(4):601–609, 1994.